Acta Oceanol. Sin., 2025, Vol. 44, No. 3, P. 102–116
https://doi.org/10.1007/s13131-025-2479-z

Effects of wind field and buoyancy fluxes on Antarctic Slope Current changes

Mingjie Ji[1, 2, 3], Ling Du[1, 2, 3*]

[1] State Key Laboratory of Physical Oceanography, Ocean University of China, Qingdao 266100, China

[2] College of Oceanic and Atmospheric Sciences, Ocean University of China, Qingdao 266100, China

[3] Frontier Science Center for Deep Ocean Multispheres and Earth System and Physical Oceanography Laboratory, Ocean University of China, Qingdao 266100, China

Received 14 October 2024; accepted 2 April 2025

© Chinese Society for Oceanography and Springer-Verlag GmbH Germany, part of Springer Nature 2025

Abstract

The Antarctic Slope Current (ASC) links the processes occurring in the coast area with the global ocean by modulating the flow across the continental slope, which influences global overturning circulation and the mass balance of the Antarctic ice shelves. This paper aims to explore the effects of wind and buoyancy fluxes on the long-term changes in the ASC using observation and reanalysis datasets. From 1993 to 2022, the ASC accelerated in all seasons, particularly in austral autumn, and was accompanied with the advancement of the strong flow. The positive buoyancy flux anomaly generates a low-density anomaly, which is accumulated by the prevailing surface easterly, maintaining a sharp density front along the continental slope. The heat flux intensifies the positive trend of buoyancy flux in summer and autumn, increasing the input of the lighter density anomaly into the ocean and advancing the strong flow of ASC. Compared with the annual mean, the additional acceleration of the ASC in autumn is mainly due to the contribution of the barotropic component, which could be explained by the local momentum input from the weakly enhanced local surface wind. The acceleration of the ASC is primarily driven by the positive trend of the buoyancy flux, while the influence of the wind on its seasonal variability becomes more significant due to the contribution of the local surface wind in autumn.

Key words polar easterly, buoyancy fluxes, long-term changes, Antarctic Slope Current (ASC)

Citation Ji Mingjie, Du Ling. 2025. Effects of wind field and buoyancy fluxes on Antarctic Slope Current changes. Acta Oceanologica Sinica, 44(3): 102–116, doi: 10.1007/s13131-025-2479-z

1 Introduction

The Antarctic Slope Current (ASC) is a counterclockwise coupled circulation and frontal system and is located on the Antarctic continental slope (Whitworth III et al., 1985; Jacobs, 1991; Thompson et al., 2018). It delineates the boundary between the cold and fresh Dense Shelf Water (DSW) and the relatively warm and salty Circumpolar Deep Water (CDW) (Carter et al., 2008) and acts as a dynamic barrier around the Antarctic continent (Jacobs, 1991). The ASC plays a pivotal role in modulating the water exchange between the shelf and the open ocean of the subpolar Southern Ocean (Thompson et al., 2018; Beadling et al., 2022). On the polar side of the ASC, the DSW has been continuously generating and migrating toward the shelf break and ultimately exporting to the open ocean (Thompson et al., 2018; Dawson et al., 2023), resulting the formation of Antarctic Bottom Water (AABW), which constitutes approximately 40% of the total volume of the global oceans (Johnson, 2008; Gordon, 2009). Furthermore, some scholars have pointed out that the ASC serves as a crucial route for iron transport in the waters around Antarctica, particularly exerting ecological effects in high chlorophyll concentration areas such as the Scotia Sea (Thompson and Youngs, 2013; Heywood et al., 2014). Even though it plays a crucial role in global climate change, our understanding of the Antarctic Slope Current remains limited and incomplete, primarily due to sparse observations and numerical models (Thompson et al., 2018; Auger et al., 2022; Beadling et al., 2022).

Foundation item: The National Natural Science Foundation of China under contract Nos 42376256, 42230405, and 41576020.
*Corresponding author, E-mail: duling@ouc.edu.cn

Due to the observation of ASC is fraught with numerous challenges (Armitage et al., 2018; Thompson et al., 2018; Pauthenet et al., 2021), it is usually not considered to be a true circumpolar circulation feature. On the western side of the Antarctic Peninsula, there is still debate regarding the presence of the ASC (Thompson et al., 2020; Huneke et al., 2022). Hence, in this study, we focused on a relatively well-defined region spanning from the western Ross Sea (170°E) to the eastern side of the Antarctic Peninsula (50°W).

The ASC is influenced by various factors such as landforms, overflow, tidal action, sea ice melting and mesoscale eddies (Meijers et al., 2010; Flexas et al., 2015; Thompson et al., 2018, 2020; Stewart et al., 2019; Moorman et al., 2020; Huneke et al., 2022), but it is most sensitive to wind stress and freshwater flux forcing (Thompson et al., 2018; Beadling et al., 2022; Cai et al., 2023). Many studies on the ASC in history have also focused on the wind and buoyancy flux along with their variations when investigating the dynamics of hydrography, circulation patterns, and cross-slope transport near the continental slope (Gill, 1973; Whitworth III et al., 1985; Jacobs, 1991; Klinck and Dinniman, 2010; Armitage et al., 2018). The seasonal cycle and variations in the ASC have been predominantly ascribed to driving by the wind fields (Gill, 1973; Mathiot et al., 2011; Yang et al., 2024). The deepening of the isopycnal toward the coast and sharpening of the baroclinicity driven by the easterly wind induces most of the seasonal variability of both the barotropic and baroclinic components of the ASC (Núñez-Riboni and Fahrbach, 2009), while the interannual variability of the ASC is related with the meridional gradient of absolute dynamic topography (ADT) which induced by the wind stress curl anomalies regulated by the southern annular mode (SAM) (Yang et al., 2024). Under global warming, the westerly winds in the Southern Hemisphere are strengthening and shifting toward the pole (Spence et al., 2014), but there is no strong evidence to support the resulting long-term change trend detected in the polar easterly winds (Hazel and Stewart, 2019; Neme et al., 2022). In addition to the changes associated with the westerly winds in the southern hemisphere and the SAM, the polar easterly winds also influenced by katabatic winds (Hazel and Stewart, 2019), particularly near the coast of the Antarctic continent (Harrison et al., 2022). Katabatic winds are generated by the cooling of the upper atmosphere over the Antarctic continent, resulting in significant meridional gradient differences at the land-sea boundary. These winds are then deflected and accelerated by the Coriolis force and gravity due to terrain constraints (Parish and Waight III, 1987), thus explaining the eastward low-level jet stream along the Antarctic coast is explained (Fulton et al., 2017). When a low-pressure system intensifies near the Antarctic coast, it can lead to an intensification of katabatic winds (Parish and Bromwich, 2007), potentially inducing stronger coastal easterly winds (Hazel and Stewart, 2019).

In the subpolar Southern Ocean, due to the significant baroclinicity of the ocean, buoyancy flux, which is dominated by salinity, also significantly affects the gyre and ASC (Snow et al., 2016; Beadling et al., 2022). In recent decades, the Antarctic ice sheet has been experiencing an accelerated volume loss (Paolo et al., 2015). Further, recent studies have indicated that this loss is not confined to the western Antarctic, which is the traditional understanding, but also extends to several regions in the eastern Antarctic which protected by the ASC (Thompson et al., 2018; Stokes et al., 2022; Wang et al., 2024). Even in recent years, the sea ice extent around the Antarctic has shown a downward trend (Hao et al., 2021). As the seawater in the subpolar region is close to the freezing point, where its coefficient of thermal expansion is close to zero (Nycander et al., 2015), the net buoyancy flux is primarily influenced by the freshwater flux (Abernathey et al., 2016; Pellichero et al., 2018). In addition, the changes in heat flux from the atmosphere are an often overlooked but important aspect of surface buoyancy flux (Snow et al., 2016). The increase in the net heat flux of the ocean under global warming is mainly attributed to downward long wave radiation (Stephens et al., 2012; Zelinka and Hartmann, 2012), which also plays a significant role in the response of the subpolar Southern Ocean to climate change (Taylor et al., 2013). Contrary to the slight changes in the easterly winds, the long-term changes in the buoyancy flux are quite evident, exhibiting a positive trend in the subpolar Southern Ocean (Pellichero et al., 2018), which further intensifies the density gradient between the shelf and open ocean, causing steepening of isopycnals at shelf break and giving the possibility of the accelerating the ASC (Snow et al., 2016; Moorman et al., 2020). As the buoyancy flux is becoming increasingly important in the subpolar Southern Ocean under the global warming, the baroclinic components of the seasonal variability of the ASC are primarily driven by the thermohaline forcing across the shelf break (Hattermann, 2018), and the accumulation of meltwater and low-density water on shelf break as a result of buoyancy flux could change the timing of the peak baroclinic component of the ASC (Lauber et al., 2024).

When a slightly strengthening wind field meets an increasing buoyancy flux field, our question naturally arises: What are their roles in the changes that the ASC is undergoing? Are they still playing the same role in these changes? The purposes of this study are to investigate the long-term changes of the ASC in the past few decades, and to answer its response to the changing surface forcing from the perspective of wind and buoyancy flux. Based on the observations and reanalysis data, we analyzed the velocity of the ASC, the polar easterly wind, and the net buoyancy flux anomaly in the subpolar Southern Ocean. In Section 2, we present the data and methods used in this paper respectively. Section 3.1 provides an overview of long-term changes in the velocity of the

ASC. Section 3.2 discusses how the buoyancy flux and wind drive the acceleration of ASC. Section 3.3 describes the dominant role of wind in additional acceleration of ASC in autumn. Finally, in Section 4, we summarize the main conclusions of this study based on the existing knowledge.

2 Data and methods

2.1 *Data*

The Global Ocean Data Analysis Project (GLODAP, v2.2023) is a synthesis activity for ocean surface to bottom data collected through analysis of water samples, and it contains data from 1 108 scientific cruises, including multiple repeated meridional cruises near the subpolar Southern Ocean (Olsen et al., 2016; Key et al., 2015). The majority of the sections of the dataset have undergone rigorous secondary quality control to ensure reliability and internal consistency, and including the systematic bias assessment (Olsen et al., 2016). Furthermore, in this paper, we reference and discuss Argo data for 2013 to 2022 as a supplement. These data were collected and made freely available by the International Argo Program and the national programs that contribute to it (https://argo.ucsd.edu, https://www.ocean-ops.org). The Argo Program is part of the Global Ocean Observing System. The floating depth of Argo floats can reach up to 2 000 × 10^4 Pa, and the average observation period is approximately 10 d (Jayne et al., 2017). Given that over 90% of the time, the Argo floats drift in accordance with the ocean currents at the designated depth, they serve as effective tools for Lagrangian observations of oceanic currents (Wong et al., 2020). The expocode of scientific cruises and the float unique identifiers of the Argo floats used in this paper are presented in Table 1.

Ocean Re-Analysis System 5 (ORAS5) is a global eddy-permitting, gridded monthly mean ocean-sea ice ensemble reanalysis system prepared by the European Centre for Medium-Range Weather Forecasts (ECMWF) (Zuo et al., 2019). This dataset, which is based on the NEMO model, incorporates subsurface temperature, salinity, sea ice intensity and sea level anomaly through the Nucleus for European Modelling of the Ocean VARiational (NEMOVAR) assimilation system, and it is forced by ECMWF Re-Analysis-Interim (ERA-Interim) atmospheric reanalysis data. In this study, the monthly temperature, salinity, current and surface flux fields were used to examine the changes in the ASC since 1993 to 2022, with a spatial resolution of 0.25° × 0.25° (equivalent to approximately 9.5 km at 70°S). The three-dimensional variables cover the entire water column from the sea surface to a depth of 5.9 km, with a total of 75 horizontal layers with unequal intervals.

The majority of the reanalyzed atmospheric data effectively captures the near-surface wind speed over the Antarctic margin and mainland. Among these, the fifth-generation ECMWF reanalysis of the global climate ECMWF Re-Analysis version 5 (ERA5) stands out due to its ability to describe the monthly averaged wind speed magnitude and the interannual variability of the near-surface wind speed (Dong et al., 2020). To assess the changes in the wind field over the subpolar Southern Ocean, this study utilizes ERA5's monthly averaged data on single levels (Hersbach et al., 2020). The variables selected are the eastward and northward components of the 10 m wind, with a spatial resolution of 0.25° × 0.25° covering a duration of 360 months from 1993 to 2022. It is important to highlight that the atmospheric variables utilized in this study differ from the forcing fields (ERA-Interim) of reanalysis datasets. The ERA-Interim data are included as a reference to ensure that these differences do not introduce errors into our analysis. Given that ECMWF has ceased the interactive download service for ERA-Interim, we sourced the monthly mean 10 m zonal wind speed for the period 1993 to 2017 from the Oceanographic Data Center, Chinese Academy of Sciences.

The sea-ice concentration (SIC) data selected in this study were obtained from the National Snow and Ice Data Center (NSIDC), and the monthly mean National Oceanic and Atmospheric Administration (NOAA)/NSIDC sea-ice concentration climate data record (CDR) data are utilized (Comiso and Nishio, 2008). The spatial resolution of the data is 25 km × 25 km. To facilitate comparison, a linear interpolation method was employed to convert the data into an Ocean Reconfigurable Computational Architecture 0.25-degree (ORCA025) mesh (0.25° horizontal resolution), which aligns with the ORAS5 in

Table 1. Expocode of the scientific cruises and the identifiers of the Argo floats

Scientific cruise	Argo float
06AQ19980328 (0°E, 1998)	7900378 (b-1, 2013)
06AQ20050122 (0°E, 2005)	7900319 (b-1, 2018)
06AQ20071128 (0°E, 2007)	5905993 (b-1, 2019)
06AQ20080210 (0°E, 2008)	7900998 (b-1, 2022)
06AQ20101128 (0°E, 2010)	7900334 (b-2, 2016)
35MFCIVA_1 (30°E, 1993)	7900934 (b-2, 2022)
35MF19960220 (30°E, 1996)	7900394 (b-3, 2015)
09AR20060102 (30°E, 2006)	7900389 (b-3, 2018)
33RR20080204 (30°E, 2008)	7900624 (b-3, 2019)
09AR19940101 (80°E, 1994)	
09AR19960119 (80°E, 1996)	
09AR20030103 (80°E, 2003)	
09AR20041223 (80°E, 2004)	
09AR20060102 (80°E, 2006)	
33RR20070204 (80°E, 2007)	
33RR20160208 (80°E, 2016)	
09AR19940101 (140°E, 1994)	
09AR19960119 (140°E, 1996)	
09AR20080322 (140°E, 2008)	
09AR20110104 (140°E, 2011)	
096U20180111 (140°E, 2018)	

the horizontal plane. The time span is from January 1993 to December 2022. This dataset exhibits minimal deviation from the observed data for Antarctica when compared to other sea ice intensity datasets (Kern et al., 2019).

2.2 *Methods*

While the zonal component of the velocity effectively represents the ASC in most regions, this zonal approximation is more suitable for relatively sparse observations. For the gridded reanalysis data, the meridional and zonal components of the velocity (represented by u, v) are usually transformed into the along-slope and across-slope velocity components and use the along-slope component of the velocity is used to more accurately characterize the flow of the ASC (Stewart et al., 2019; Huneke et al., 2022; Yang et al., 2024). The along-slope component of velocity (u_{along}) is derived from the projection of the tangent to the velocity of climatological state of the ASC within the Cartesian coordinate system. $\mathcal{S}_{\text{ASC}}$ represents the climate trajectory curve of the ASC.

$$u_{\text{along}} = (u, v) \cdot \left[\frac{\partial_y \mathcal{S}_{\text{ASC}}}{|\nabla \mathcal{S}_{\text{ASC}}|} - \frac{\partial_x \mathcal{S}_{\text{ASC}}}{|\nabla \mathcal{S}_{\text{ASC}}|} \right]. \tag{1}$$

We assumed that the Argo floats maintain a constant velocity in a straight trajectory along the horizontal plane at their working depths during the intervals between their ascent to the surface for signal transmission, and that the sole driving force behind the horizontal displacement is ocean currents (Park et al., 2005). Based on the Lagrangian measurements, in order to conduct a simple estimation of the flow velocity of the Argo floats drifting (u_{argo}), we assumed that the flow velocity is equal to the drifting displacement (ΔL) is divided by the time interval (Δt):

$$u_{\text{argo}} = \frac{\Delta L}{\Delta t}. \tag{2}$$

A narrow belt of easterly winds is set over the Antarctic continental margin in order to emphasize the effect of the wind on the changes of the ASC. In the study area, the local surface wind is defined as the wind at a height of 10 m within a latitude range of 2° north and south of the Antarctic slope. Characterized by the contour representing the minimum wind speed, the wind field in the subpolar Southern Ocean is classified into northern westerlies and southern polar easterlies. However, these contours do not consistently lie on the northern side of the continental slope and intersect land at the Antarctic Peninsula (Neme et al., 2022). Consequently, to concentrate on the effect of the local surface winds on the ASC, the northern boundary for local wind is established at 2° north of the shelf break, which coinciding closely with the contours representing minimum wind speed in the climatological state. Meanwhile, the southern boundary is set at 2° south of the continental shelf break, approximately coincides the coastline. In this paper, the eastward winds are defined as negative values of zonal winds in accordance with established conventions.

The freshwater and heat fluxes are combined to obtain the net surface buoyancy flux:

$$B_{\text{net}} = \frac{g}{\rho} \left[\alpha \frac{F_{\text{h}}}{C_{\text{p}}} + \beta (F_{\text{fw}} S_0) \right], \tag{3}$$

where F_{h} and F_{fw} denote the net surface heat flux and surface freshwater flux, g is the acceleration due to gravity (9.8 m/s²), ρ is the density of seawater (1.027×10^3 kg/m^3), α is the coefficient of thermal expansion (3.529×10^{-5} K^{-1}), C_{p} is the specific heat capacity of seawater [3.89×10^3 (kg·J)/m^3], β is the shrinkage coefficient of brine (7.846×10^{-4} kg/g), and S_0 is the sea surface salinity from the ORAS5 reanalysis data.

In this paper, we used multiple linear regression analysis to discuss the quantitative relationship between buoyancy flux, wind, and ASC. Pearson correlation is used to estimate the degree of similarity between the time series. In this study, the multi-year monthly trend and the long-term trends are all classified as the long-term changes.

3 Results and discussion

3.1 *Long-term changes of Antarctic Slope Current*

Figure 1a illustrates the average zonal velocity in the subpolar Southern Ocean during 1993–2022, as well as the climatological state location of the ASC. The solid line delineates the ASC region of concern in this paper. The four green solid lines labeled with Roman numerals indicate the locations of the GLODAP scientific cruise sections, and the three black fan-shaped boxes denote the tracks of Argo floats in Figs 1a and b.

Both the observations and the reanalysis data indicate an acceleration of the ASC. Due to the proximity of the ASC to the continental shelf, the complex terrain and sea ice cause all of the flow axes from the scientific cruise sections to be predominantly located at or slightly beyond the southernmost part of each section (Fig. 2a). These zonal component of the baroclinic geostrophic currents is computed using the thermohaline. The velocity of the ASC increases from east to west, reaching its maximum velocity at 0° (the Weddell Sea) and minimum velocity at 140°E (the Dumont d'Urville Sea) (Table 2). While the velocity variation characteristics near the continental slope differ across the sections, the trend of westward acceleration is universal except for at 140°E (Fig. 2a). The reanalysis data for the aforementioned sections, demonstrate that the acceleration occurred during 1993 to 2022 in all of these sections. The strongest accelerating occurred in the South Atlantic Ocean, and the trend in the southern Indian Ocean is relatively weak (Fig. 2b). In conclusion, the observation and reanalysis data indicate that in most regions of the east Antarctic margin, the ASC exhibited a strengthening trend. However, it should be noted that be-

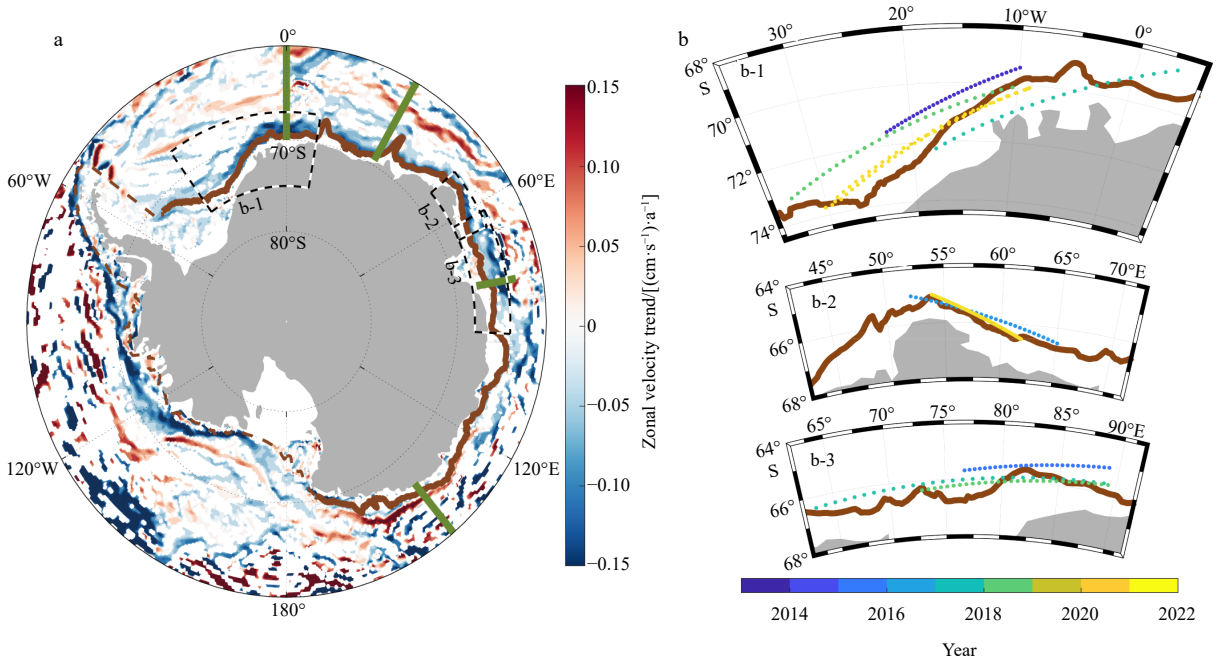


Fig. 1. Zonal velocity trends and locations of the measured data for the subpolar Southern Ocean from 1993 to 2022 (a), and tracks of Argo floats that approximately form repeated sections in the subpolar Southern Ocean between 2013 to 2022 (b). The shading in a indicates that the trend at this grid passes the 95% confidence test, the brown line represents the climatological location of the ASC, and the green solid line denotes the GLODAP scientific cruise sections. The trajectory of the Argo floats (b-1, b-2, and b-3) correspond to the three fan-shaped boxes in a.

Table 2. Velocity and trend of the ASC in mixed layer at different sections

Longitude (corresponding sea area)	Velocity[1)]/(cm·s^{-1})			Trend[4)]/[(cm·s^{-1})/a]		
	GLODAP	ORAS5[2)]	Zonal mean[3)]	GLODAP	ORAS5	Zonal mean
0° (Weddell Sea)	–21.1	–16.2	–9.6	–0.17	–0.13**	–0.08**
30°E (Cosmonaut Sea)	–14.9	–8.5	–8.6	–0.24	–0.10**	–0.07**
80°E (Prydz Bay)	–13.2	–11.5	–7.1	–0.41	–0.03**	–0.04*
140°E (Dumont d'Urville Sea)	–12.9	–7.5	–6.9	0.16	–0.04**	–0.05*

Note: [1)]The depth averaged flow in the mixing layer, positive represents eastward. [2)]The temporal range of the average and trend values of the reanalysis data presented in this table corresponds to the period during which all observed data for the same section were collected. [3)]Based on ORAS5 reanalysis, the zonal mean from the regions in heading parentheses. [4)]Due to the relatively sparse observed data, all trends calculated based on observed data are not suitable for confidence test, while **(*) represents passing the 95% (90%) confidence test.

cause the observations are relatively sparse, the analysis of the long-term trends may be disturbed by seasonal changes, and exist errors due to sensitivity to the length of data.

The ASC is accelerating in all seasons, particularly in austral autumn. Figure 3 provides a more detailed representation of the ASC velocity from the ORAS5 reanalysis data. During 1993 to 2022, the average flow velocity in the mixed layer in the ASC is measured at –7 cm/s, with a negative trend of –0.04 (cm·s^{-1})/a (passing the 95% confidence test). Except for the Southeast Indian Ocean sector, the velocity trend of the ASC is almost consistent above 2 000 m (Fig. 3a). The trend exhibits strong baroclinicity vertically, and the contribution of the geostrophic component explains about 51% of the overall trend in the mixed layer (Fig. 3b). The average flow velocity in the mixed layer in the ASC accelerate in most months, and the most significant acceleration occurs in austral autumn (March–May) which is also the strongest season in the ASC (Fig. 3c). The average flow velocity in the upper 2 000 m is –4 cm/s, and there is also a weak accelerated trend [–0.02 (cm·s^{-1})/a, passing the 95% confidence test]. At the depth of 2 000 m, the seasonal cycle and the multi-year monthly trend of ASC are similar to those in the mixed layer; however, the trend of velocity passing the 95% confidence test is only occurred during autumn (not be shown). The significant accelerating in autumn increases the seasonal range of ASC. The black solid line in Fig. 3d represents the seasonal variations in the ASC flow velocity, which is calculated as the absolute value of the difference between the strongest (autumn) and the weakest (spring) seasons, indicating a strengthening trend

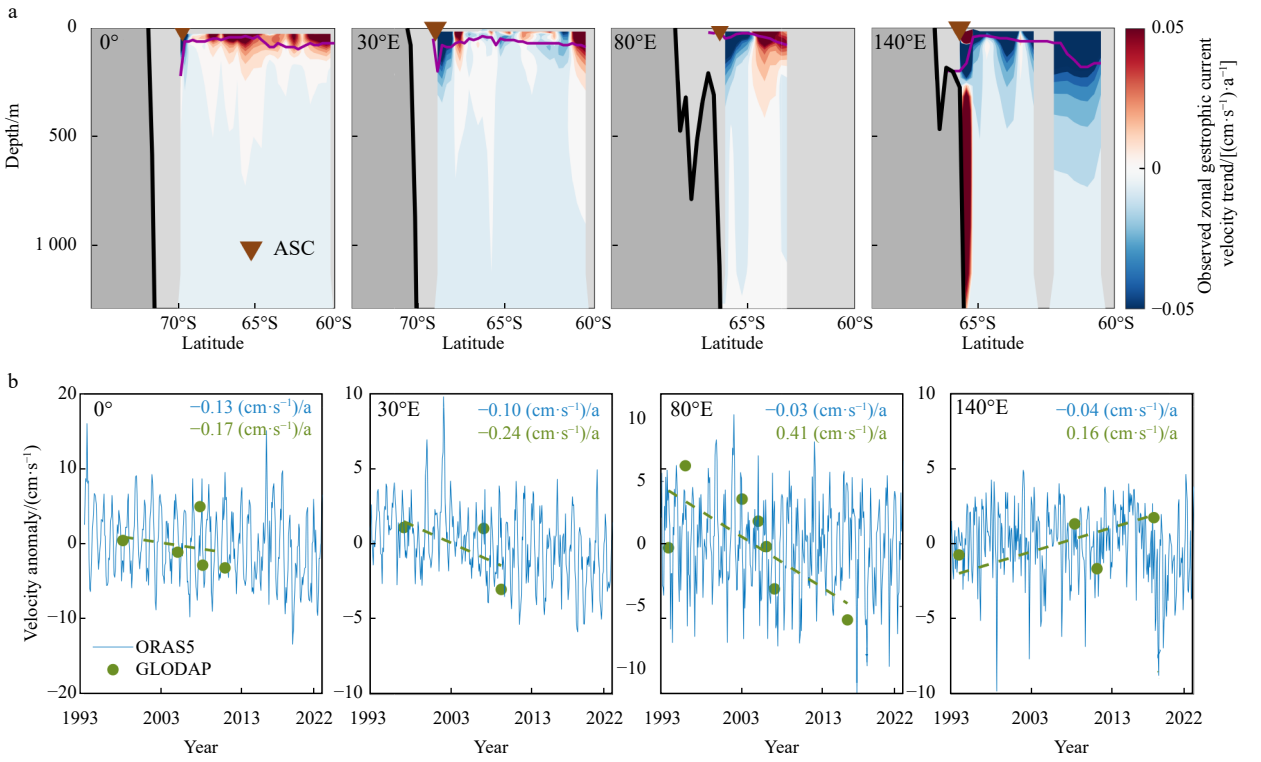


Fig. 2. Observed zonal geostrophic current velocity trends from the four GLODAP cruise sections (shading) (a), with the seabed topography (solid black line) and the climatological location of ASC (brown triangle), and light gray shaded area represent missing measured values; the velocity anomalies of ASC derived from observations and reanalysis data in different sections (b). In b, blue line indicates ORAS5 and green dot indicates GLODAP.

[0.03 (cm·s^{-1})/a, passing the 95% confidence test]. The event that deviates from the mean by one standard deviation (gray shaded area represents the one standard deviation from the mean seasonal range on left axis) in the flow velocity time-series is classified as an anomaly of the seasonal range (Fig. 3d). The red (blue) solid circles indicate abnormal events that are above (below) the mean, and their corresponding years are referred to as strong (weak) flow years. After 2017, the strong flow years have occurred frequently; while the weak flow years mainly occurred before 2003, with only one occurrence in 2013. Furthermore, compared with the acceleration of the annual, the additional acceleration in autumn is mainly manifested as significant barotropic feature (Fig. 3b).

The occurrence of strong flow is advancing earlier. The maximum monthly mean velocity of the ASC occurs in May, with the flow velocity can reach –8 cm/s in the mixed layer, while the minimum monthly mean velocity occurs in December and is –5 cm/s (Fig. 3c). In this paper, the maximum ASC velocity in the seasonal cycle is called strong flow, while the minimum velocity is called weak flow. The ASC not only exhibits a significant accelerating trend in autumn but the month of strong flow occurrence advances at a rate of 1 month per decade (passing the 95% confidence test). Between 1993 and 2001, the median month for the occurrence of maximum velocity was July. From 2014 to 2022, the median occurrence time of the strong flow has shifted to May, advancing by approximately two months (Fig. 4). Simultaneously, there is virtually no discernible changes in the advance or lag of the month in which the ASC occurs its weak flow velocity (Fig. 4), as well as statistically significant trend.

Furthermore, as a supplement to the scientific cruises, in this study, we utilized data for the Argo floats that measured repeated sections in the subpolar Southern Ocean between 2013 to 2022 (Fig. 1b). According to their drifting tracks, the Lagrange method can be used to calculate their drifting velocities, which are considered to approximate the flow of the ASC during the observation period of the floats. Compared with the other two datasets, the velocities measured by the Argo floats are found to be slower, and the highest velocity observed in Prydz Bay instead of the Weddell Sea (Table 3). In addition, the Argo floats also observed the velocity of ASC exhibited an accelerating towards the west.

3.2 *Acceleration of the ASC is driven by buoyancy flux and local surface wind*

The acceleration of ASC could be attributed to the effects of the local surface wind enhancement and the positive trend of net buoyancy flux. Due to the long-term change of ASC flow velocity is most significant in autumn. Consequently, this study focuses on comparing the differences in wind and buoyancy fluxes in autumn between the strong and weak flow years. There is a significant correlation between the velocity of ASC in autumn

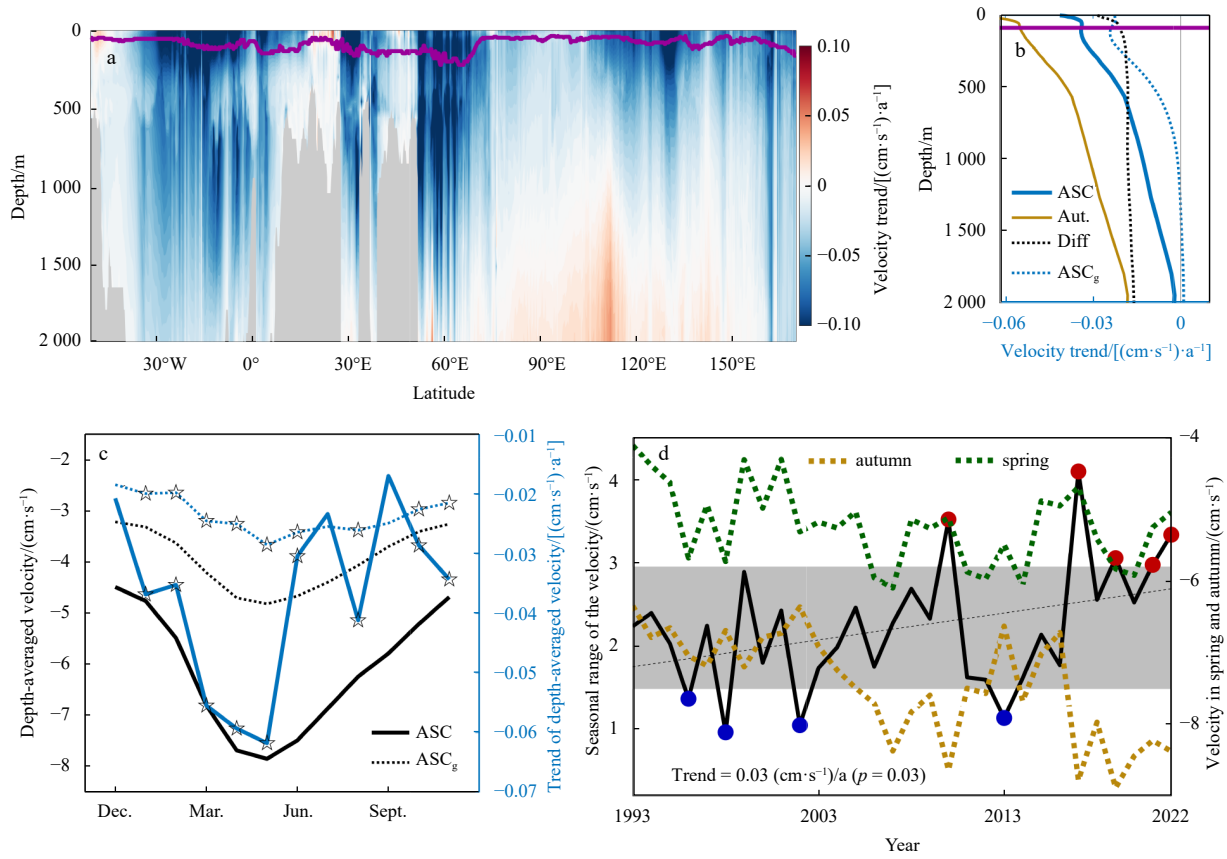


Fig. 3. Zonal and vertical spatial distributions of velocity trend of the ASC velocity during 1993–2022 (a); vertical velocity feature of the ASC (b); the seasonal cycle (black) and multi-year monthly trends (blue) of the flow velocity average in the mixed layer of the ASC (dashed: geostrophic) (c); the seasonal range of the velocity of the ASC (black solid line) and the flow velocity in spring (green dashed line) and autumn (yellow dashed line) (d). In a, the purple line represents the mixed layer depth. In b, the blue solid (dashed) line represents the annual mean total (geostrophic) flow, and the black dashed line represents the difference between the trend in autumn (gold solid line) and the annual mean (blue solid line). In c, the pentagrams on the blue line indicate that the trend for the month has passed the 95% confidence test. In d, the gray dashed line indicates a linear trend, and the gray shaded area represents the one standard deviation from the mean seasonal range.

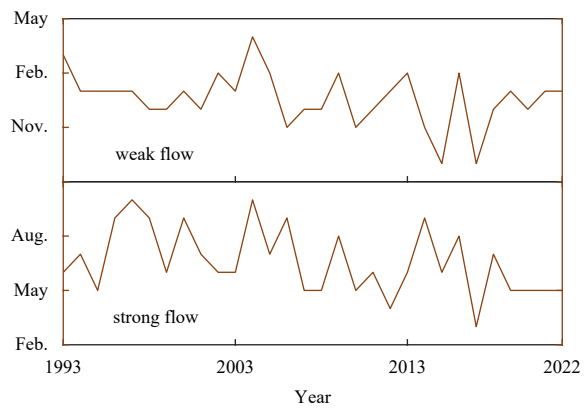


Fig. 4. Occurrence month of ASC weak flow velocity and strong flow velocity.

and the local surface wind speed as well as the heat flux (Fig. 5a). Through composite analysis, it is found that the heat flux (local surface wind) exhibits a significant positive anomaly (negative anomaly) in the years when the

Table 3. Flow velocity and trend of Antarctic Slope Current observed by Argo floats

Area	Velocity/(cm·s^{-1})	Trend/[(cm·s^{-1})/a]
Eastern Weddell Sea (b-1)	–6.0	–0.42
West side of Cape Darnley (b-2)	–5.9	–0.26
Outside Prydz Bay (b-3)	–7.9	–0.97

Note: b-1, b-2, and b-3 correspond to the sea areas marked in Fig. 2a.

seasonal range exceeds one standard deviation from the mean. Conversely, these features will reverse when the seasonal variation falls below the mean (Figs 5b and c). By comparing the local surface wind and heat flux during autumn under these two types of seasonal range anomalies, it is found that the Weddell Sea, the Prydz Bay and the Dumont d'Urville Sea are the key areas where the heat flux is most significant, while the Weddell Sea, the Cos-

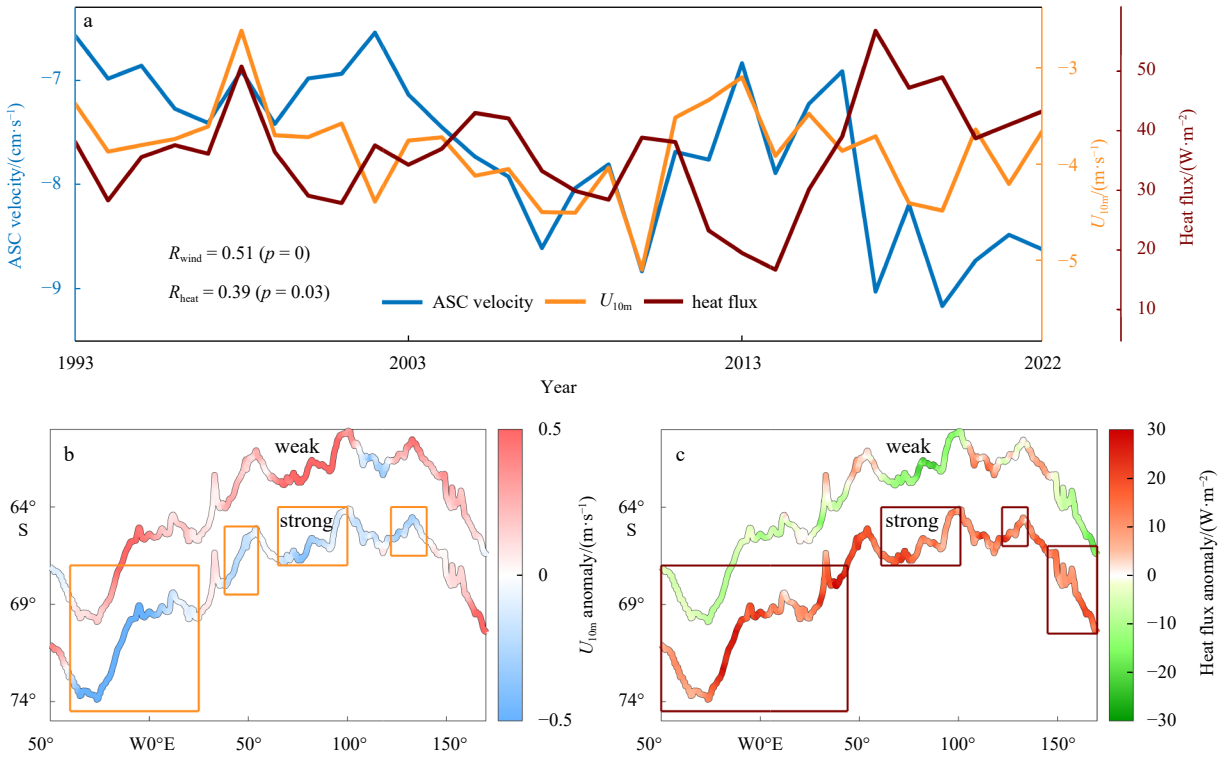


Fig. 5. Velocity of ASC (light blue), local surface wind speed (U_{10m}, yellow) and heat flux in buoyancy (maroon) in autumn during 1993 to 2022 (a), and the local surface wind speed (U_{10m}) anomaly (b) and heat flux anomaly (c) during the period with an abnormal seasonal amplitude. In b and c, the orange and red boxes highlight the key areas with the most significant changes in local surface wind and heat flux during years of anomalous seasonal range in velocity.

monaut Sea and the Southern Indian Ocean sector are the key areas of the local surface wind.

Local surface wind is anticipated to exhibit a weak enhancement during austral autumn, with the area of enhancement showing high spatial consistency with key areas identified through the corresponding composite analysis. Figure 6a illustrates the specific spatial range of the local surface wind that effects on the ASC. There are spatially heterogeneous variations in the local surface wind near the shelf break, with the weak enhancement in easterly winds over the Atlantic sector and a decrease over the Indian Ocean sector (Fig. 6b). Focusing on autumn specif-

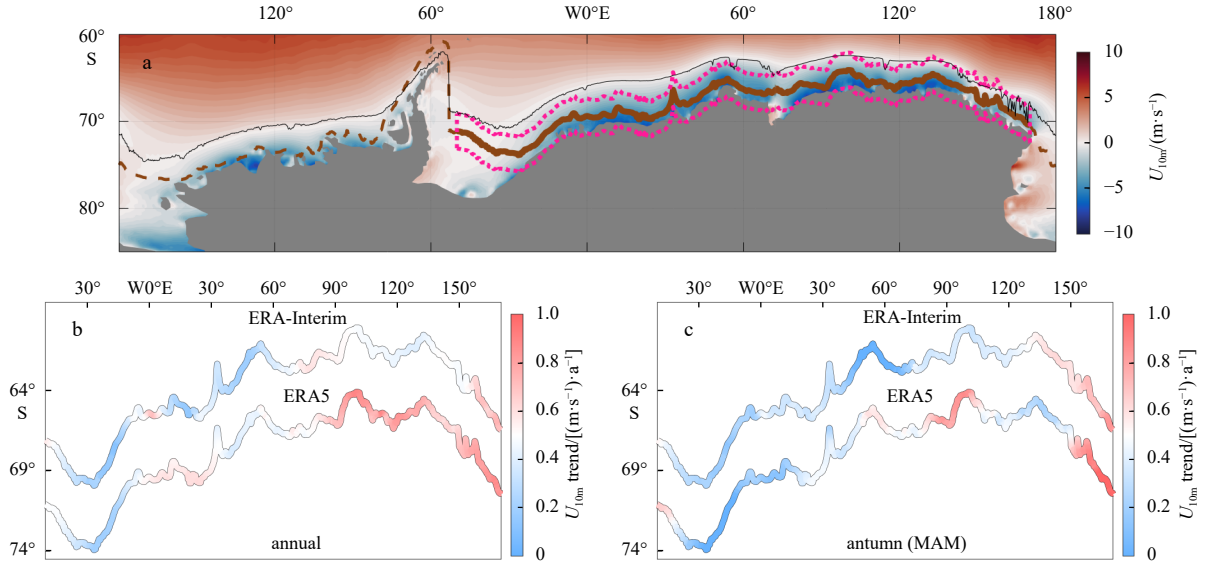


Fig. 6. Spatial range of the local surface wind in this study (magenta dotted line), with the wind speed (U_{10m}, shading), ASC (brown line), and the contour line of the minimum wind speed (black thin solid line) (a); trends of local surface wind speed along the shelf break in annual mean (b) and austral autumn (c). The latitude recorded on the vertical axis corresponds only to the bottom curve (ERA5), and the curve shape represents the flow axis of the ASC.

ically, the local surface wind intensifies from the Weddell Sea to the Cosmonaut Sea west of 40°E, with a weak strengthening trend also observed in the Dumont d'Urville Sea (Fig. 6c). Additionally, the enhancement of the easterly wind over the Weddell Sea may persist from spring to autumn, while the most significant enhancement of the easterly wind on the Prydz Bay mainly occurs in winter (not be shown). The results of ERA-Interim support the ERA5-based findings regarding the easterly wind trends, despite the minor differences in data length (ERA-Interim covers only 1993 to 2017), suggesting that the influence of the local surface winds on the ASC is genuine instead of model errors. Enhanced local surface wind not only accelerate ASC by directly inputting momentum into the ocean, but also contribute to that by facilitating the baroclinic adjustment process in the ocean via Ekman transport.

In addition to changes in the local surface wind, the wind stress curl field along the Antarctic continental margin in the southeastern Indian Ocean sector could generate significant positive anomalies during the positive phase of the SAM. These anomalies also reduce the meridional sea surface height gradient near the slope (Armitage et al., 2018; Auger et al., 2022), to suppress the acceleration of the geostrophic circulation of the ASC, thereby influencing the three-year significant period in the interannual variability of ASC velocity (not be shown).

The buoyancy flux exhibits an overall positive trend in the subpolar Southern Ocean, with the areas displaying the positive trend of heat flux showing a high spatial consistency with key areas identified through the corresponding composite analysis. The previous section discussed the significant baroclinic characteristics of the acceleration in the ASC, and the geostrophic component plays a significant role in it (Fig. 3). Therefore, the change of buoyancy flux is concerned in this study as it significantly influences the density field variations near the slope. In the subpolar Southern Ocean, the buoyancy flux anomaly is generally influenced by the contribution of the freshwater flux and exhibits an overall positive trend (Fig. 7a). In the austral autumn, when the acceleration of the ASC reaches its peak, the contribution of the heat flux becomes particularly pronounced and dominates the spatial variations in the buoyancy flux near the shelf break. Figure 7b shows the trends of the buoyancy flux, freshwater flux, and heat flux in autumn within the same spatial range. The spatial distribution of the trend of the freshwater flux near the shelf break is relatively consistent, whereas the heat flux exhibits a significant positive trend in the eastern Weddell Sea, the Cosmonaut Sea, and the Dumont d'Urville Sea, which are same as the key areas in Fig. 5b. The spatial difference characteristics of the net surface buoyancy flux trend near the continental slope is dominated by the heat flux in autumn, which modulates the spatial characteristics of the ASC acceleration.

The buoyancy flux induces baroclinic adjustments through the introduction of low-density anomalies into the ocean, dominating the acceleration of the ASC and advancing the strong flow. The season variations in the buoyancy flux near the shelf break within a range of 2° to the north and south from 1993 to 2022 are depicted in Fig. 8a. In terms of the seasonal cycle, there are two peaks in the buoyancy flux in December and March. The strongest peak in the buoyancy flux occurs in December. This is closely associated with the melting of the sea ice in summer and primarily is driven by the freshwater flux. In contrast, the peak in March, which is dominated by the heat flux, is a sub-peak within the seasonal cycle and mainly resulting from the expansion of the open ocean following the melting of the sea ice in summer, which promotes the absorption of heat from the atmosphere by the ocean. Figure 8b illustrates the monthly trends of the buoyancy flux. There are two evident peaks in summer (January) and autumn (April), and the peak value in summer almost equal to that in autumn, about 1.3 $(W \cdot m^{-2})/a$ (passing the 95% confidence test). The trend of the heat

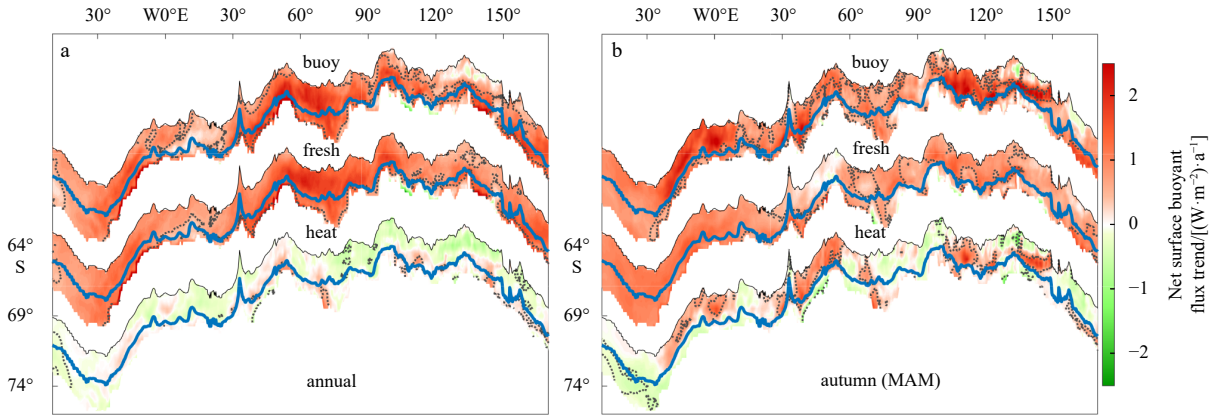


Fig. 7. Trends of the net surface buoyant flux near the Antarctic shelf break in annual mean (a) and austral autumn (b). The blue solid lines represent the location of ASC, and the gray dashed lines are the contours that pass the 95% confidence test. The latitude recorded on the vertical axis corresponds only to the bottom shading (corresponded by the heat in subplot), and the position of other shadows is obtained by shifting the bottom shading up by 6° in latitude in turn. MAM: March, April, and May.

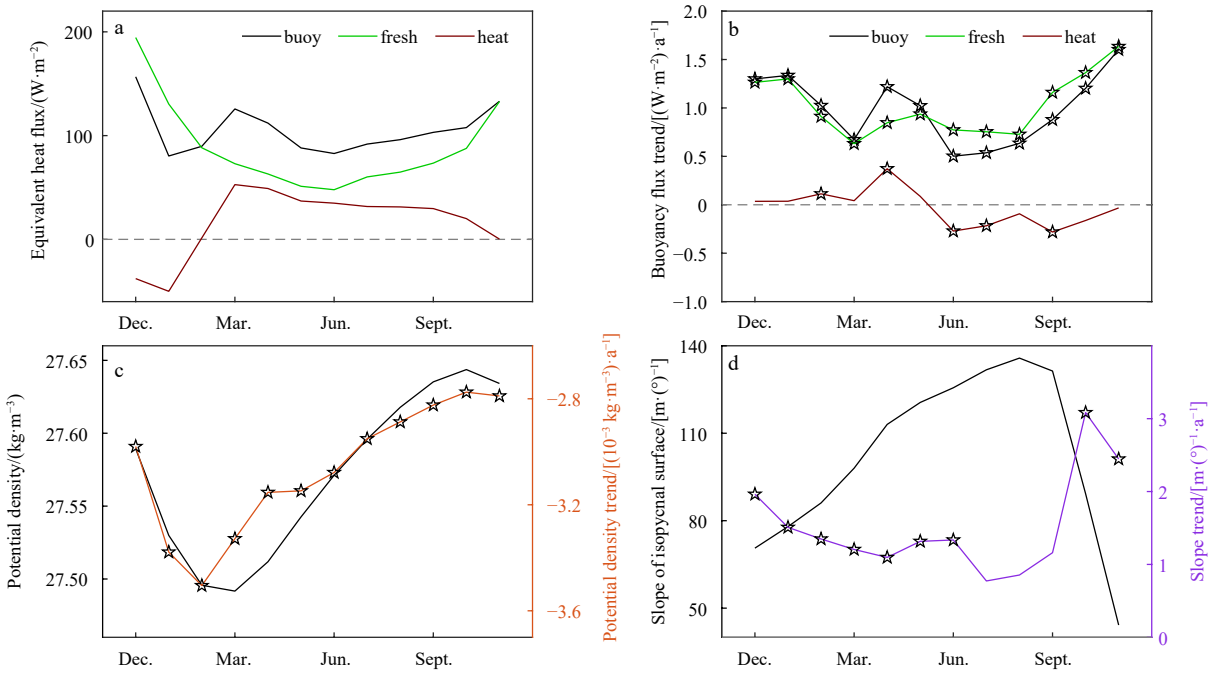


Fig. 8. Seasonal cycle (a) and multi-year monthly trends (b) of the buoyancy flux, seasonal cycle and multi-year monthly trends of the potential density in the mixed layer south of the ASC (c), and slope of the isopycnal surface (27.6 kg/m^3) (d). The pentagrams on the colored solid line represent the trend for the month has passed the 95% confidence test.

flux is positive in summer and autumn, and negative in winter and spring. This seasonal reversal of the trend of the heat flux further amplifies the positive trend of the buoyancy flux in summer and autumn. Although the net buoyancy flux near the ASC is primarily influenced by the freshwater flux, it is essential to acknowledge the significant contribution of the heat flux in autumn (Figs 7, 8a and b), particularly pronounced in shaping its spatial characteristics. The buoyancy flux in the key region shown in Fig. 5c exhibits the strongest correlation (0.50) with the ASC velocity lagged by one month (synchronous correlation coefficient is 0.44). Additionally, the occurrence of the maximum acceleration of the ASC in the seasonal cycle also lags behind the peak lightening of the density induced by buoyancy flux variations during the seasonal cycle. Dynamically, the positive trend of the buoyancy flux has introduced more low-density anomalies into the ocean, which accumulate onshore under the influence of prevailing easterly winds over the continental slope, ultimately resulting in a significant lightening of the potential density in the mixed layer south of the slope (Fig. 8c). And these processes steepen the isopycnal surface near the slope leading to the baroclinic adjustment, which accelerated the ASC (Fig. 8d), while simultaneously explain the lag of the velocity trend relative to the buoyancy flux trend. Meanwhile, due to the significant low-density trend in the mixed layer south of the slope in summer and autumn, the slope of the isopycnal surface continues to become steeper during the same period, and advancing the strong flow of ASC by promoting the baroclinic adjustment. The low-density anomalies entering the ocean will continue to increase and accumulate across the seasons near the slope, leading to a steeper trend in late winter (October, Fig. 8d), prolonging the period of isopycnal surface is steep.

While the contributions of the local surface wind and the buoyancy flux to ASC are significant, it does not imply that the ASC is solely influenced by these factors (Thompson et al., 2018). To comprehensively assess potential contributions from other factors to the long-term change of the ASC, we established a multiple linear regression model incorporating several standardized factors based on the previous researches (Meijers et al., 2010; Thompson et al., 2018, 2020; Stewart et al., 2019; Moorman et al., 2020; Huneke et al., 2022): the buoyancy flux (B), the local surface wind (W), the topography effect (P), the dense water overflow (D), the sea ice concentration (C), and the southern annual model index (SAM). The terms B, W, S, and SAM represent the timeseries or index of the corresponding factors, respectively. D denotes the maximum potential density within each grid water column where bottom density exceeding 27.8 kg/m^3 on the continental slope, while the P corresponds to the timeseries of potential vorticity at the slope. Finally, we obtain a predictive equation that passing the regression testing, and the coefficient of determination (R^2) is 0.54:

$$Z = (-0.658\,3\,B + 0.434\,1\,W + 0.214\,3\,D - 0.079\,6\,C) \times U_{\mathrm{std}} + \overline{U}, \tag{4}$$

where Z at the left of the Eq. (4) is the prediction of the ASC velocity, while the U_{std} and $\overline{U}$ represent the variance

and mean of the velocity timeseries, respectively. During the regression analysis, we filtered out the seasonal variations of the aforementioned factors and found that both the topography and SAM contributed minimally to the ASC velocity, neither of which passed the confidence test. This may be attributed to the fact that topographic influences on the ASC primarily in morphological and spatial characteristics (Baines, 2009), while the influence of SAM on the ASC are predominantly seasonal (Armitage et al., 2018; Auger et al., 2022) and interannual. The overflow enhances oceanic stratification by restricting the downward transport of the cooling and freshening, generating a meridional density gradient with lower (higher) value in the north (south), thereby suppressing the geostrophic velocity of the westward ASC. However, the overflow is limited by the spatially constrained, occurring in the dense shelf where the DSW exists. Additionally, in areas of anomalously increased winter sea ice along the East Antarctica, the sea ice concentration modulates the ASC by impeding the response of ocean to atmospheric momentum input processes, acting more as a damping effect rather than an active dynamic process. Therefore, we attribute the acceleration of the ASC to the result of the local surface wind and buoyancy flux, especially the contribution of buoyancy flux.

3.3 *Local surface wind causes the additional acceleration of ASC in austral autumn*

However, the seasonal variation of low-density anomaly at the slope caused by buoyancy flux is not exactly the same as ASC (Figs 3 and 8), especially the low-density anomaly cannot explain the additional acceleration of the ASC in autumn. In Fig. 9a, a depiction is presented for multi-year monthly mean speeds of the local surface winds at 10 m, as well as their trends. The black line denotes the multi-year monthly mean of the local surface winds. Meanwhile, the orange solid line illustrates trends for local surface winds spanning from 1993 to 2022 in different months calculated by ERA5, while the orange dashed line is from the ERA-Interim (1993 to 2017) (Fig. 9a). Months passing the 75% confidence test are marked by black hollow pentagrams. The multi-year monthly trend of the wind speed from ERA-Interim data is highly similar to that from the ERA5 data, and the obtained seasonal variations in the wind trend are nearly identical, particularly during autumn and winter. The results from ERA5 and ERA-Interim strengthen the confidence in the phenomenon of the weak enhancement of the local surface wind in autumn. The multi-year monthly trends of the wind speed are depicted in Fig. 9a, only March, April, June, and September passing the 75% confidence test; none passing the 95% confidence test, which further underscores the complexities associated with the polar easterly alterations. By comparing the meridional gradient of the 1 000 hPa geopotential height between the Antarctic coast and the subpolar trough, we infer that the primary positive trend of the Katabatic wind occurs in autumn (April and May, Fig. 9b). Therefore, the enhance-

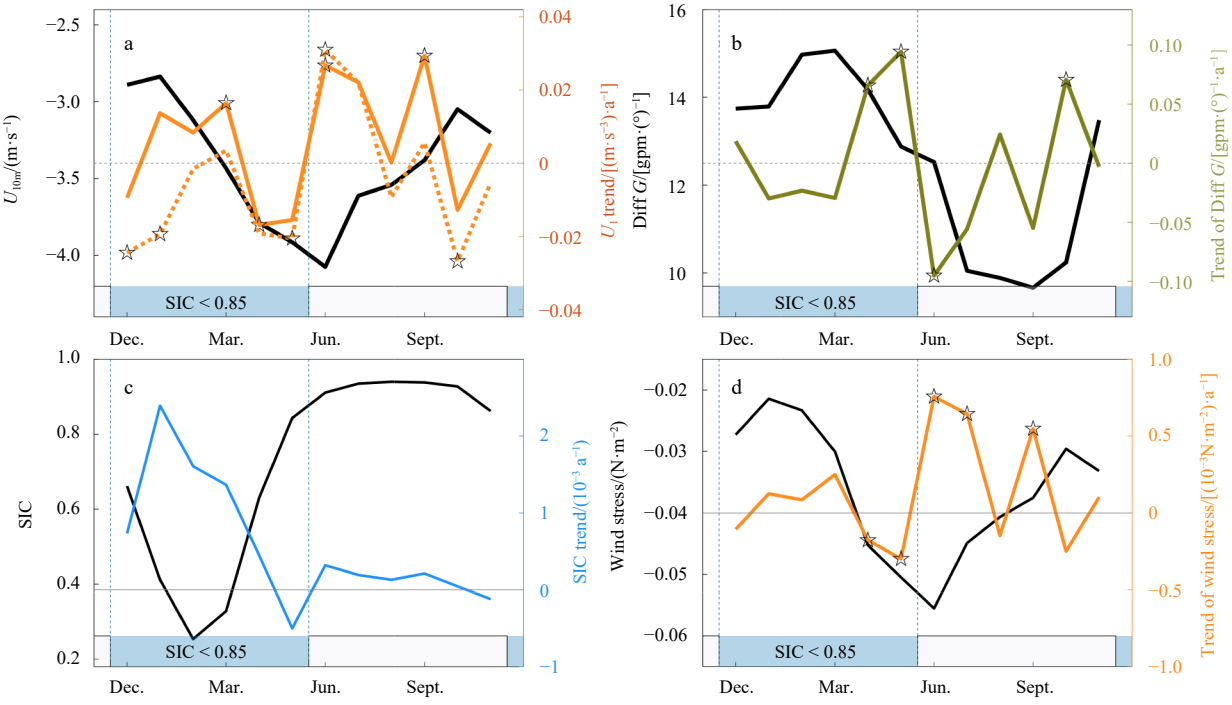


Fig. 9. Seasonal cycle and multi-year monthly trends of the local surface wind speed (U_{10m}, a) (solid line: ERA5, dashed line: ERA-Interim), the meridional gradient of the 1 000 hPa geopotential height (Diff G, b), the SIC (c) and the wind stress (d). The blue (white) shading below the images indicates that the SIC in the month is below (above) 0.85. The pentagram on the colored solid line represents the trend for the month passes the 75% confidence test. In b, gpm is the abbreviation for geopotential meter.

ment of local surface wind in autumn could be attributed to the positive anomaly trend of the meridional gradient of the geopotential height over the Antarctic continental margin. Moreover, it is certain that the local zonal wind speed can reach 4.0 m/s in June and 2.8 m/s in January, indicating the easterly wind which driving the ASC is still robust.

Local surface wind accelerates the ASC by increasing the direct momentum input to the ocean, and explains the most significant characteristics of the flow trend of the ASC in autumn from the barotropic perspective. Firstly, Fig. 9c shows the seasonal cycle of SIC and its multi-year monthly trend in the range of 2° north and south of the Antarctic shelf break. The seasonal variations in SIC play an important role in the effect of local surface wind on ASC, as the open water resulting from sea ice melting facilitates the wind momentum transfer to the ocean during strong easterly wind, whereas high SIC hinders the response of ocean to the weakening easterly wind. Slight variations in the long-term change of SIC have kept this period relatively stable. Since polar easterlies are strongest and stronger in autumn (April−May; Fig. 9a), although this does not correspond exactly to the period of the open water, changes in the zonal wind stress near the slope suggest that the stronger easterlies are still able to input more momentum directly into the ocean (Fig. 9d). The synchronous correlation coefficient between autumn wind speed and the time series of the flow velocity average in the mixed layer can reach 0.39 (p = 0.03). Especially in the eastern Weddell Sea and the Cosmonaut Sea, where easterly intensities are most significant (Fig. 6). In the flow field, the average depth flow is usually taken as the barotropic component, while the momentum input of the wind to the ocean greatly affects the barotropic flow on the slope (Núñez-Riboni and Fahrbach, 2009; Auger et al., 2022). The long-term trend of ASC in autumn is the most significant, and its additional acceleration compared to the annual mean is also mainly characterized by barotropic (Fig. 3b). Therefore, while buoyancy flux dominates the annual mean acceleration of the ASC, the additional acceleration of ASC in autumn is attributed to the barotropic adjustment caused by local surface wind.

4 Conclusions

In this study, observation reanalysis data are used to examine the effects of the local surface wind and net buoyancy flux anomaly on the long-term changes of the ASC. Over the past 30 years, the average flow velocity in the mixed layer in the ASC increased by approximately 1 cm/s, i.e., about 10% of the climatological mean velocity. Based on the seasonal variations in the long-term changes, the acceleration of ASC is most pronounced during austral autumn. The trend is nearly twice as much as the annual mean (Fig. 3c) and significantly contributing to the increase in seasonal range (Fig. 3d). The additional acceleration of ASC in autumn, compared with the trend of the annual mean, is mainly characterized by barotropic (Fig. 3b). Furthermore, the strong flow of the ASC is advancing, by about 2 months over the statistical time period (Fig. 4).

The surface forcing that dominates the acceleration of ASC is the buoyancy flux rather than the wind, and the positive trend of the buoyancy flux predominantly controls the acceleration of the ASC and the advancement of the strong flow. The positive buoyancy flux introduces the formation of a lighter density anomaly in the ocean, leading to the accumulation of lighter density signals on the shelf and potential density loss in the mixed layer south of the slope (Fig. 8c). It subsequently increases the baroclinicity (Fig. 8d) and ultimately accelerates the ASC. Regression analysis demonstrates that the buoyancy flux term explains 55% of the variance in the predicted variable and contributes 56% to the value of flow velocity trends (Table 4). The net surface buoyancy flux is primarily influenced by freshwater flux, while the contribution of heat flux cannot be overlooked in seasonal cycle (Figs 8a and b). In spring and summer, heat flux further strengthens the positive trend of the buoyancy flux (Fig. 8b), leading to advancement of baroclinic adjustment process induced by the buoyancy flux and the early occurrence of strong flow. Additionally, the geostrophic component of the ASC does not exhibit sharp acceleration during autumn (Fig. 3c), which implies that this trend may be attributed to non-geostrophic components such as the local surface wind.

There are closely related between the most significant acceleration of the ASC in austral autumn and the local surface wind, which further enhances the dominant role of the wind on the seasonal cycle and variation of the ASC. The additional acceleration of the ASC in autumn comes mainly from the contribution of local surface winds, and the additional trend caused by local surface wind increases significantly more than the buoyancy flux in autumn (Table 4). The local surface wind exhibits the most substantial contribution to the velocity trend of the ASC dur-

Table 4. Contribution of each factor to the velocity in the mixed layer in the ASC

Statistical metric	Period	Contribute to the velocity			
		Buoyancy	Local surface wind	Overflow	Sea ice concentration
Value of trend[1] /[(cm·s^{-1})/a]	annual	56% (−0.027)	26% (−0.013)	–7% (0.003)	2% (−0.001)
	autumn[2]	46% (−0.034)	39% (−0.023)	5% (−0.003)	1% (−0.001)
Variance	annual	29%	19%	5%	2%

Note: [1] The proportion of the corresponding term in the flow velocity in the mixed layer in the ASC, which minus the seasonal variation. The numbers in parentheses are specific values. [2] Include March, April, and May.

ing autumn, accounting for 39% of the velocity trend value, which significantly surpasses the annual average of 26%. The easterly wind slightly enhancement is mainly concentrated in the Weddell Sea, the Cosmonaut Sea, and the Southeast Indian Ocean sector in autumn (Fig. 6). The local surface wind which is dominated by the meridional gradient between the Antarctic coast and the subpolar trough, exhibits only a slightly acceleration of the trend of less than 0.2 ($m \cdot s^{-1}$)/a (passing the 75% confidence test) in April and May. Due to the relatively low SIC in autumn, the enhanced local surface wind inputs of more momentum to the ocean, leading to the ASC accelerates most significantly in autumn, and explaining the barotropic character of the additional acceleration of ASC in autumn. In addition, the wind stress curl field affected by the SAM also influence the three-year period of the interannual variation in the ASC by modulating the sea surface height gradient.

From the perspective of wind and buoyancy flux, we try to explain the response mechanism of the ASC to changing surface forcing in the long-term changes. It is hypothesized that global warming will bring more positive buoyancy flux anomalies in subpolar Southern Ocean in the future, which will further promote the acceleration of ASC. This speculation may contribute to improve the understanding of the less sensitivity of the East Antarctic ice sheet to climate change from circulation perspective. As a critical dynamical barrier along the Antarctic continental slope, a stronger ASC would likely suppress cross-slope intrusions of CDW while inducing significant subsurface cooling over the continental shelf. Furthermore, with the continued warming of the Southern Ocean, the reduction in sea ice cover may not only enhance wind-driven momentum transfer to the ocean but also intensify tidal mixing processes, facilitating exchanges between CDW and shelf water and altering the density driven mechanism of the ASC (Thompson et al., 2018). However, it should be noted that this study is rather idealistic as it averages the entire ASC while ignoring detailed differences brought about by different shelf types along the way, and does not consider the connection between the ASC and the rest sectors of the subpolar Southern Ocean.

Acknowledgement

Besides the datasets and institutions mentioned in the "Data" section, the authors would like to thank the data support from Oceanographic Data Center, Chinese Academy of Sciences (https://www.casodc.com/).

References

Abernathey R P, Cerovecki I, Holland P R, et al. 2016. Water-mass transformation by sea ice in the upper branch of the Southern Ocean overturning. Nature Geoscience, 9(8): 596–601, doi: 10.1038/ngeo2749

Armitage T W K, Kwok R, Thompson A F, et al. 2018. Dynamic topography and sea level anomalies of the Southern Ocean: variability and teleconnections. Journal of Geophysical Research: Oceans, 123(1): 613–630, doi: 10.1002/2017JC013534

Auger M, Sallée J B, Prandi P, et al. 2022. Subpolar Southern Ocean seasonal variability of the geostrophic circulation from multi-mission satellite altimetry. Journal of Geophysical Research: Oceans, 127(6): e2021JC018096, doi: 10.1029/2021JC018096

Baines P G. 2009. A model for the structure of the Antarctic Slope Front. Deep-Sea Research Part Ⅱ: Topical Studies in Oceanography, 56(13–14): 859–873, doi: 10.1016/j.dsr2.2008.10.030

Beadling R L, Krasting J P, Griffies S M, et al. 2022. Importance of the Antarctic Slope Current in the Southern Ocean response to ice sheet melt and wind stress change. Journal of Geophysical Research: Oceans, 127(5): e2021JC017608, doi: 10.1029/2021JC017608

Cai Wenju, Gao Libao, Luo Yiyong, et al. 2023. Southern Ocean warming and its climatic impacts. Science Bulletin, 68(9): 946–960, doi: 10.1016/j.scib.2023.03.049

Carter L, McCave I N, Williams J M. 2008. Chapter 4 circulation and water masses of the Southern Ocean: a review. Developments in Earth and Environmental Sciences, 8: 85–114

Comiso J C, Nishio F. 2008. Trends in the sea ice cover using enhanced and compatible AMSR-E, SSM/I, and SMMR data. Journal of Geophysical Research: Oceans, 113(C2): C02S07

Dawson H R S, Morrison A K, England M H, et al. 2023. Pathways and timescales of connectivity around the Antarctic continental shelf. Journal of Geophysical Research: Oceans, 128(2): e2022JC018962, doi: 10.1029/2022JC018962

Dong Xu, Wang Yetang, Hou Shugui, et al. 2020. Robustness of the recent global atmospheric reanalyses for Antarctic near-surface wind speed climatology. Journal of Climate, 33(10): 4027–4043, doi: 10.1175/JCLI-D-19-0648.1

Flexas M M, Schodlok M P, Padman L, et al. 2015. Role of tides on the formation of the Antarctic slope front at the Weddell-Scotia confluence. Journal of Geophysical Research: Oceans, 120(5): 3658–3680, doi: 10.1002/2014JC010372

Fulton S R, Schubert W H, Chen Zhengqing, et al. 2017. A dynamical explanation of the topographically bound easterly low-level jet surrounding Antarctica. Journal of Geophysical Research: Atmospheres, 122(23): 12635–12652

Gill A E. 1973. Circulation and bottom water production in the Weddell Sea. Deep-Sea Research and Oceanographic Abstracts, 20(2): 111–140, doi: 10.1016/0011-7471(73)90048-X

Gordon A L. 2009. Bottom water formation. In: Steele J H, Thorpe K K, Thorpe S A, eds. Ocean Currents. London: Academic Press, 263–269

Hao Guanghua, Shen Hui, Sun Yongming, et al. 2021. Rapid

decrease in Antarctic sea ice in recent years. Acta Oceanologica Sinica, 40(7): 119–128, doi: 10.1007/s13131-021-1762-x

Harrison T C, Biri S, Bracegirdle T J. et al. 2022. Reanalysis representation of low-level winds in the Antarctic near-coastal region. Weather and Climate Dynamics, 3(4): 1415–1437, doi: 10.5194/wcd-3-1415-2022

Hattermann T. 2018. Antarctic thermocline dynamics along a narrow shelf with easterly winds. Journal of Physical Oceanography, 48(10): 2419–2443, doi: 10.1175/JPO-D-18-0064.1

Hazel J E, Stewart A L. 2019. Are the near-Antarctic easterly winds weakening in response to enhancement of the Southern Annular Mode?. Journal of Climate, 32(6): 1895–1918

Hersbach H, Bell B, Berrisford P, et al. 2020. The ERA5 global reanalysis. Quarterly Journal of the Royal Meteorological Society, 146(730): 1999–2049, doi: 10.1002/qj.3803

Heywood K J, Schmidtko S, Heuzé C, et al. 2014. Ocean processes at the Antarctic continental slope. Philosophical Transactions of the Royal Society A, 372(2019): 20130047, doi: 10.1098/rsta.2013.0047

Huneke W G C, Morrison A K, Hogg A M. 2022. Spatial and subannual variability of the Antarctic Slope Current in an eddying ocean–sea ice model. Journal of Physical Oceanography, 52(3): 347–361, doi: 10.1175/JPO-D-21-0143.1

Jacobs S S. 1991. On the nature and significance of the Antarctic Slope Front. Marine Chemistry, 35(1–4): 9–24, doi: 10.1016/S0304-4203(09)90005-6

Jayne S R, Roemmich D, Zilberman N, et al. 2017. The Argo program: present and future. Oceanography, 30(2): 18–28, doi: 10.5670/oceanog.2017.213

Johnson G C. 2008. Quantifying Antarctic bottom water and North Atlantic deep water volumes. Journal of Geophysical Research: Oceans, 113(C5): C05027

Kern S, Lavergne T, Notz D, et al. 2019. Satellite passive microwave sea-ice concentration data set intercomparison: closed ice and ship-based observations. The Cryosphere, 13(12): 3261–3307, doi: 10.5194/tc-13-3261-2019

Key R M, Olsen A, van Heuven S, et al. 2015. Global ocean data analysis project, version 2 (GLODAPv2). Oak Ridge: Carbon Dioxide Information Analysis Center, Oak Ridge National Laboratory, U. S. Department of Energy

Klinck J M, Dinniman M S. 2010. Exchange across the shelf break at high southern latitudes. Ocean Science, 6(2): 513–524, doi: 10.5194/os-6-513-2010

Lauber J, de Steur L, Hattermann T, et al. 2024. Observed seasonal evolution of the Antarctic Slope Current system off the coast of Dronning Maud Land, East Antarctica. Journal of Geophysical Research: Oceans, 129(4): e2023JC020540, doi: 10.1029/2023JC020540

Mathiot P, Goosse H, Fichefet T, et al. 2011. Modelling the seasonal variability of the Antarctic Slope Current. Ocean Science, 7(4): 455–470, doi: 10.5194/os-7-455-2011

Meijers A J S, Klocker A, Bindoff N L, et al. 2010. The circulation and water masses of the Antarctic shelf and continental slope between 30 and 80°E. Deep-Sea Research Part Ⅱ: Topical Studies in Oceanography, 57(9–10): 723–737, doi: 10.1016/j.dsr2.2009.04.019

Moorman R, Morrison A K, Hogg A M. 2020. Thermal responses to Antarctic ice shelf melt in an eddy-rich global ocean–sea ice model. Journal of Climate, 33(15): 6599–6620, doi: 10.1175/JCLI-D-19-0846.1

Neme J, England M H, Hogg A M. 2022. Projected changes of surface winds over the Antarctic continental margin. Geophysical Research Letters, 49(16): e2022GL098820, doi: 10.1029/2022GL098820

Núñez-Riboni I, Fahrbach E. 2009. Seasonal variability of the Antarctic Coastal Current and its driving mechanisms in the Weddell Sea. Deep-Sea Research Part Ⅰ: Oceanographic Research Papers, 56(11): 1927–1941, doi: 10.1016/j.dsr.2009.06.005

Nycander J, Hieronymus M, Roquet F. 2015. The nonlinear equation of state of sea water and the global water mass distribution. Geophysical Research Letters, 42(18): 7714–7721, doi: 10.1002/2015GL065525

Olsen A, Key R M, van Heuven S, et al. 2016. The Global Ocean Data Analysis Project version 2 (GLODAPv2)—an internally consistent data product for the world ocean. Earth System Science Data, 8(2): 297–323, doi: 10.5194/essd-8-297-2016

Paolo F S, Fricker H A, Padman L. 2015. Volume loss from Antarctic ice shelves is accelerating. Science, 348(6232): 327–331, doi: 10.1126/science.aaa0940

Parish T R, Bromwich D H. 2007. Reexamination of the near-surface airflow over the Antarctic continent and implications on atmospheric circulations at high southern latitudes. Monthly Weather Review, 135(5): 1961–1973, doi: 10.1175/MWR3374.1

Parish T R, Waight III K T. 1987. The forcing of Antarctic katabatic winds. Monthly Weather Review, 115(10): 2214–2226, doi: 10.1175/1520-0493(1987)115<2214:TFOAKW>2.0.CO;2

Park J J, Kim K, King B A, et al. 2005. An advanced method to estimate deep currents from profiling floats. Journal of Atmospheric and Oceanic Technology, 22(8): 1294–1304, doi: 10.1175/JTECH1748.1

Pauthenet E, Sallée J B, Schmidtko S, et al. 2021. Seasonal variation of the Antarctic slope front occurrence and position estimated from an interpolated hydrographic climatology. Journal of Physical Oceanography, 51(5): 1539–1557, doi: 10.1175/JPO-D-20-0186.1

Pellichero V, Sallée J B, Chapman C C, et al. 2018. The Southern Ocean meridional overturning in the sea-ice sector is driven by freshwater fluxes. Nature Communications, 9(1): 1789, doi: 10.1038/s41467-018-04101-2

Snow K, Hogg A M, Sloyan B M, et al. 2016. Sensitivity of Antarctic Bottom Water to changes in surface buoyancy fluxes. Journal of Climate, 29(1): 313–330, doi: 10.1175/JCLI-D-15-0467.1

Spence P, Griffies S M, England M H, et al. 2014. Rapid sub-

surface warming and circulation changes of Antarctic coastal waters by poleward shifting winds. Geophysical Research Letters, 41(13): 4601–4610, doi: 10.1002/2014GL060613

Stephens G L, Wild M, Stackhouse Jr P W, et al. 2012. The global character of the flux of downward longwave radiation. Journal of Climate, 25(7): 2329–2340, doi: 10.1175/JCLI-D-11-00262.1

Stewart A L, Klocker A, Menemenlis D. 2019. Acceleration and overturning of the Antarctic Slope Current by winds, eddies, and tides. Journal of Physical Oceanography, 49(8): 2043–2074, doi: 10.1175/JPO-D-18-0221.1

Stokes C R, Abram N J, Bentley M J, et al. 2022. Response of the East Antarctic Ice Sheet to past and future climate change. Nature, 608(7922): 275–286, doi: 10.1038/s41586-022-04946-0

Taylor P C, Cai Ming, Hu Aixue, et al. 2013. A decomposition of feedback contributions to polar warming amplification. Journal of Climate, 26(18): 7023–7043, doi: 10.1175/JCLI-D-12-00696.1

Thompson A F, Speer K G, Chretien L M S. 2020. Genesis of the Antarctic Slope Current in west Antarctica. Geophysical Research Letters, 47(16): e2020GL087802, doi: 10.1029/2020GL087802

Thompson A F, Stewart A L, Spence P, et al. 2018. The Antarctic Slope Current in a changing climate. Reviews of Geophysics, 56(4): 741–770, doi: 10.1029/2018RG000624

Thompson A F, Youngs M K. 2013. Surface exchange between the Weddell and Scotia Seas. Geophysical Research Letters, 40(22): 5920–5925, doi: 10.1002/2013GL058114

Wang Chuning, Zhang Zhaoru, Zhong Yisen, et al. 2024. A model study of buoyancy driven cross-isobath transport over the Ross Sea continental shelf break. Journal of Geophysical Research: Oceans, 129(1): e2023JC020078, doi: 10.1029/2023JC020078

Whitworth Ⅲ T, Orsi A H, Kim S J, et al. 1985. Water masses and mixing near the Antarctic Slope Front. In: Jacobs S S, Weiss R F, eds. Ocean, Ice, and Atmosphere: Interactions at the Antarctic Continental Margin. Washington: American Geophysical Union, 1–27

Wong A P S, Wijffels S E, Riser S C, et al. 2020. Argo Data 1999–2019: Two million temperature-salinity profiles and subsurface velocity observations from a global array of profiling floats. Frontiers in Marine Science, 7: 700, doi: 10.3389/fmars.2020.00700

Yang Shikai, Zhou Meng, Cheng Xuhua. 2024. Seasonal and interannual variability between upper ocean processes and the slope current in the region around the Cosmonauts Sea off east Antarctica. Journal of Geophysical Research: Oceans, 129(2): e2023JC019636, doi: 10.1029/2023JC019636

Zelinka M D, Hartmann D L. 2012. Climate feedbacks and their implications for poleward energy flux changes in a warming climate. Journal of Climate, 25(2): 608–624, doi: 10.1175/JCLI-D-11-00096.1

Zuo Hao, Balmaseda M A, Tietsche S, et al. 2019. The ECMWF operational ensemble reanalysis–analysis system for ocean and sea ice: a description of the system and assessment. Ocean Science, 15(3): 779–808, doi: 10.5194/os-15-779-2019